nature chemical biology

ARTICLES

https://doi.org/10.1038/s41589-019-0284-8

Light-based control of metabolic flux through assembly of synthetic organelles

Evan M. Zhao[1], Nathan Suek[1], Maxwell Z. Wilson[2], Elliot Dine[2], Nicole L. Pannucci[2], Zemer Gitai[2], José L. Avalos[1,3*] and Jared E. Toettcher[2*]

To maximize a desired product, metabolic engineers typically express enzymes to high, constant levels. Yet, permanent pathway activation can have undesirable consequences including competition with essential pathways and accumulation of toxic intermediates. Faced with similar challenges, natural metabolic systems compartmentalize enzymes into organelles or post-translationally induce activity under certain conditions. Here we report that optogenetic control can be used to extend compartmentalization and dynamic control to engineered metabolisms in yeast. We describe a suite of optogenetic tools to trigger assembly and disassembly of metabolically active enzyme clusters. Using the deoxyviolacein biosynthesis pathway as a model system, we find that light-switchable clustering can enhance product formation six-fold and product specificity 18-fold by decreasing the concentration of intermediate metabolites and reducing flux through competing pathways. Inducible compartmentalization of enzymes into synthetic organelles can thus be used to control engineered metabolic pathways, limit intermediates and favor the formation of desired products.

Metabolic engineering aims to divert cellular metabolites to a desired biosynthetic pathway with the goal of maximizing a product of interest[1]. This goal is usually pursued by manipulating expression levels: overexpressing the enzymes required for product formation and reducing enzyme expression in competing, endogenous pathways[2,3]. However, expressing an engineered pathway at constant, high levels can face numerous challenges. Diverting flux to engineered pathways may compete with essential natural pathways, necessitating the use of small-molecule inducers to turn enzyme expression on at a particular time or to an intermediate level[4]. Furthermore, the level of overexpression needed for efficient product generation can itself be deleterious due to the burden of synthesizing these high enzyme loads[5]. Considerable advantages could thus be gained by increasing flux through an engineered pathway on demand without altering enzyme expression levels, yet few examples exist of post-translational, dynamic regulation of metabolic flux in metabolic engineering[6–9].

In contrast, dynamic, post-translational regulation is a hallmark property of natural metabolisms[10–12]. Cells can shift metabolic flux in response to diverse signals by redistributing existing enzymes into co-localized clusters[13] or membrane-bound organelles[14] without changing total enzyme quantities (Fig. 1a–c). Previous theoretical and experimental work also provides a mechanistic explanation for clustering-induced metabolic flux: when sequential enzymes in a pathway are co-localized, the product of the first enzyme can have a high probability of reaction through the second enzyme before diffusing away from the cluster[15]. An additional consequence of this mechanism is more efficient conversion of intermediate metabolites, lowering their steady-state concentrations. This effect can be crucial for limiting intermediates that are toxic at high concentrations[16] or preventing loss to alternative, branched pathways[8,9,15].

Due to these advantages, the idea of engineering synthetic organelles to co-localize the components of an engineered metabolism has gained considerable interest in recent years. Recent studies have achieved increased product yields by localizing metabolic enzymes to synthetic scaffolds[17,18], encapsulins[19], the host cell's mitochondria[20], peroxisomes[21] and other organelles[22], as well by expressing enzyme fusion proteins that aggregate into higher-order clusters[15]. However, no approaches yet exist to trigger the assembly or disassembly of these synthetic structures on demand to enable fast, reversible control over metabolic flux.

Optogenetics offers a potential solution to this challenge. Light can be applied and removed at will, enabling dynamic, reversible control over protein interactions[23]. Moreover, we and others have established a suite of tools for optogenetic control over protein clustering in live cells[24–26]. Here, we report that light-controlled clustering can be extended to the assembly of functional metabolic organelles. Starting from the recently published optoDroplet and PixELL systems[24,25], we developed methods for obtaining yeast strains in which protein clusters could be reliably assembled and dissolved. Using the deoxyviolacein pathway as a model metabolic pathway, we find that synthetic co-localization of sequential enzymes can enhance metabolic flux in a light-switchable manner. Light-regulated clustering leads to a 6.1 ± 0.9-fold change in the level of the desired product, achieving the theoretical maximum expected fold change for two-enzyme co-localization[15], as well as an 18-fold increase in selectivity over an alternative, non-enzymatic product. The programmable assembly/disassembly of membraneless organelles thus offers a new strategy for rapid post-translational dynamic control of engineered metabolic pathways.

Results

Optogenetic clustering can be variable between cells. We set out to reversibly control metabolic flux in microbes using a set of recently developed optogenetic clustering tools[24–27]. Many light-induced clustering approaches are based on the *Arabidopsis thaliana* Cry2 photolyase homology domain (henceforth termed Cry2) that oligomerizes on blue light stimulation[28]. Cry2 oligomerization can

[1]Department of Chemical and Biological Engineering, Princeton University, Princeton, NJ, USA. [2]Department of Molecular Biology, Princeton University, Princeton, NJ, USA. [3]Andlinger Center for Energy and the Environment, Princeton University, Princeton, NJ, USA. *e-mail: javalos@princeton.edu; toettcher@princeton.edu

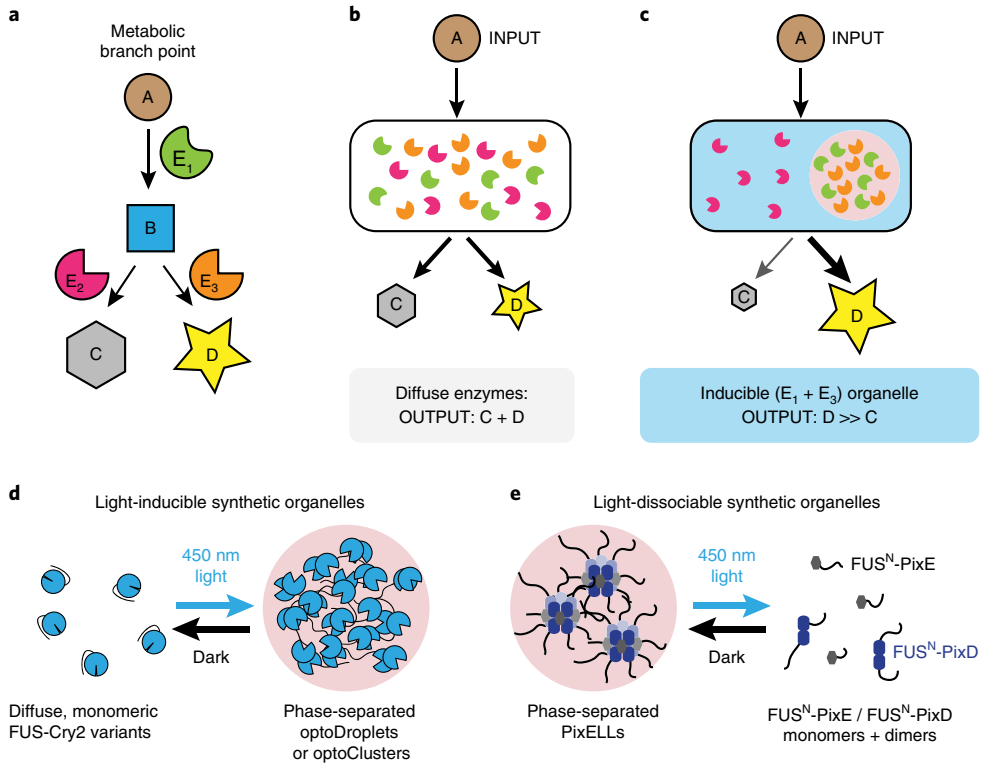

Fig. 1 | Light-switchable synthetic organelles for redirecting metabolic flux. a, A schematic of metabolic flux in a branched pathway. Metabolites A, B, C and D are converted through the action of enzymes E_1, E_2 and E_3. **b**, Under conditions in which E_3 and E_2 are similarly efficient, metabolite B will be converted to mixture of products C and D. **c**, Synthetic metabolic organelles can bias flux at branch points: by co-localizing enzymes $E_1 + E_3$, B will be shunted toward product D, thereby limiting production of the unwanted byproduct C. **d**,**e**, Two general strategies for optogenetic regulation of membraneless organelle assembly. FUS^N fusions to variants of the Cry2 optogenetic system lead to light-induced protein phase separation in the optoDroplet and optoCluster systems (**d**), whereas FUS^N fusions to the PixD/E proteins form the light-dissociable PixELL optogenetic system (**e**).

be enhanced by a point mutation (in a variant termed Cry2olig)[26] as well as by fusion to the N terminal intrinsically disordered region (IDR) from the protein FUS (FUS^N)[24]. Both FUS^N-Cry2 and FUS^N-Cry2olig fusion proteins exhibit rapid, reversible clustering in mammalian cells (Fig. 1d) with different physical properties: FUS^N-Cry2 forms liquid-like spherical droplets that rapidly exchange monomers in and out of clusters, whereas FUS^N-Cry2olig forms rigid clusters that do not exchange subunits with the solution[24]. Throughout this study, we will refer to these systems as optoDroplets and optoClusters, respectively (Fig. 1d).

We also tested an additional optogenetic clustering system with an inverted light response termed the PixELL system[25]. PixELLs are based on the PixD and PixE proteins from *Synechocystis* sp. PCC6803. PixD and PixE form a high-order complex in the dark that dissociates into PixE monomers and PixD dimers after blue light stimulation[29]. We previously found that IDR fusions of these two proteins (FUS^N-PixD and FUS^N-PixE) form liquid-like droplets when co-expressed in mammalian cells, and that these droplets are rapidly disassembled within seconds on blue light illumination[25] (Fig. 1e).

We began by adapting optoDroplets for expression in *Saccharomyces cerevisiae* by constructing a 2μ plasmid containing a fusion of FUS^N, the FusionRed fluorescent protein[30] and Cry2 (Fig. 2a). We observed light-dependent changes in oligomerization of this fusion protein in some cells, suggesting that the optoDroplet system is indeed functional in yeast. However, the quality of light-induced droplet formation was variable from cell to cell. Many cells failed to assemble droplets on light stimulation; in others, droplets remained assembled even in the dark (Fig. 2a and Supplementary Fig. 1a). We hypothesized that this heterogeneity was due to cell-to-cell variability in gene expression caused by differences in 2μ plasmid copy number. A strong dependence of clustering on expression level is to be expected from the principles of phase separation. If the protein concentration is too low, even maximum illumination will fail to induce clustering, whereas if it is too high, the intrinsic tendency for FUS^N to aggregate will dominate even in the dark[24]. The kinetics of droplet assembly may also exhibit substantial concentration-dependent differences[24,25,31]. This cell-to-cell variability in droplet formation is a barrier to adopting light-regulated synthetic organelles for metabolic engineering.

A selection strategy for obtaining homogenous clustering. To overcome cell-to-cell variability in droplet formation, we set out to find ideal protein levels for light-induced organelle assembly, while also obtaining homogeneous responses in most cells in a colony. We turned to a genome integration and selection strategy using the antibiotic zeocin. A useful feature of zeocin resistance is that it is highly dose-dependent, so increasing zeocin levels selects for increasing Zeo^R expression[32]. We thus hypothesized that by genomically integrating a variable number of zeocin-resistant optogenetic cassettes and replica-plating the transformed cells on plates containing different zeocin concentrations, we would be able to reproducibly obtain strains at optoDroplet expression levels that support light-switchable droplet formation in all cells within a colony (Supplementary Fig. 1b).

We built cassettes for expression of either the optoDroplet or optoCluster systems driven by the medium-strength P_{ADH1} promoter as well as a zeocin resistance marker (plasmid pNS1 and pNS3, see Supplementary Table 1), and integrated variable numbers of copies of the construct into δ-sites of the yeast genome as

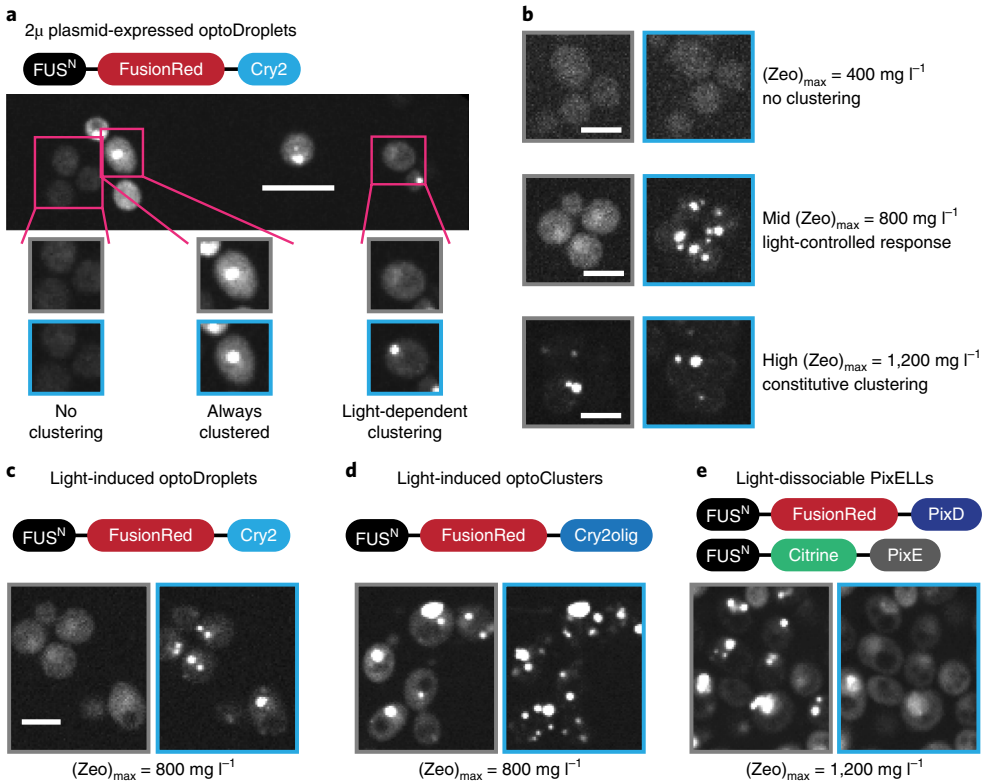

Fig. 2 | Light-regulated organelle formation depends on component concentration. a, A strain expressing optoDroplets from a 2μ plasmid (strain YEZ53) exhibits three different clustering responses in the same colony. Low-expressing cells fail to cluster in all illumination conditions, high-expressing cells remain clustered and only a small portion of cells reversibly form clusters with light. Representative images of four independent experiments are shown. Scale bar, 10 μm. **b**, Zeocin selection of multiply integrated constructs enables titration of expression levels without increasing cell-to-cell variability in clustering (strain YNS47). Colonies show no organelle formation at the maximum concentration of zeocin in which a colony can grow, termed $[Zeo]_{max} = 400\ mg\ l^{-1}$ (left), light-inducible organelle formation at $[Zeo]_{max} = 800\ mg\ l^{-1}$ (middle) and constitutive organelle formation at $[Zeo]_{max} = 1{,}200\ mg\ l^{-1}$ (right). Scale bars, 5 μm. **c**–**e**, FusionRed fluorescence for three optogenetic systems in the presence or absence of blue light: optoDroplets (strain YNS47, **c**), optoClusters (strain YNS49, **d**) and PixELLs (strain YEZ232, **e**). Blue boxes indicate images acquired after cells were incubated in blue light, gray boxes indicate images acquired after dark incubation. Images in **c**–**e** are identically scaled; scale bar in **c**, 5 μm.

previously described[32]. We plated transformed cells onto a nonselective plate for a short outgrowth (see Methods for details), followed by replica-plating at a series of zeocin concentrations. To estimate the expression levels of individual transformants, we define a quantity $[Zeo]_{max}$ as the maximum concentration of zeocin in which a colony can grow (Supplementary Fig. 1b). Previous genomic analysis of similar constructs indicated that a $[Zeo]_{max}$ of $400\ mg\ l^{-1}$ corresponds to 1–2 copies, a $[Zeo]_{max}$ of $800\ mg\ l^{-1}$ corresponds to 3–4 copies and a $[Zeo]_{max}$ of $1{,}200\ mg\ l^{-1}$ corresponds to 5–6 copies[33]. We observed that $[Zeo]_{max}$ was predictive of optogenetic system expression and photoswitchable droplet formation (Fig. 2b). In colonies with $[Zeo]_{max}$ of $400\ mg\ l^{-1}$, we observed low expression and poor droplet formation (Fig. 2b, top). At the other extreme, colonies with $[Zeo]_{max}$ of $1{,}200\ mg\ l^{-1}$ exhibited constitutive droplets and high expression (Fig. 2b, bottom). For colonies with intermediate $[Zeo]_{max}$ values, robust photoswitchable droplet formation was consistently observed (Fig. 2b, center).

To further characterize the dynamics and reversibility of photoswitchable organelle formation, we selected optoDroplet and optoCluster colonies with a $[Zeo]_{max}$ of $800\ mg\ l^{-1}$ and imaged FusionRed localization by confocal microscopy in response to sequences of darkness and blue illumination (Fig. 2c,d and Supplementary Videos 1 and 2)[24,26]. The inclusion of the IDR tag was crucial, as strains expressing FusionRed-Cry2 or FusionRed-Cry2olig without the FUS^N tag failed to exhibit robust clustering at any $[Zeo]_{max}$ level (Supplementary Fig. 1c,d). We found that optoDroplets exhibited the cleanest change from diffuse to clustered localization on light stimulation (Fig. 2c). In contrast, optoClusters exhibited some clusters in un-illuminated cells but also exhibited more overall redistribution into clusters on illumination (Fig. 2d). This is consistent with previous observations that Cry2olig shows an increased propensity to cluster compared to Cry2 (ref. [26]).

We obtained similar results with the inverse PixELL system. On the basis of the observation that PixELL clusters contain PixD and PixE in a 2:1 stoichiometry[34], we first integrated a single copy of FUS^N-Citrine-PixE driven by the P_{PGK1} promoter into the *HIS3* locus, and then integrated a variable number of copies of P_{ADH1}–driven FUS^N-FusionRed-PixD into δ-sites (YEZ232, Supplementary Tables 1 and 2). Colonies having $[Zeo]_{max}$ of $1{,}200\ mg\ l^{-1}$ exhibit robust PixD/PixE clustering that dissociate after blue light stimulation (Fig. 2e and Supplementary Video 3). As expected, both PixD and PixE constructs were required for clustering, as strains expressing only one or the other showed only diffuse localization (Supplementary Fig. 1e,f).

We further validated that optoDroplets, optoClusters and PixELLs are each functional in two yeast strains commonly used in cell biology and metabolic engineering studies, BY4741 (refs. [35,36]) and CEN.PK2-1C[37] (for BY4741, see Supplementary Fig. 2 and for CEN.PK2-1C, see Fig. 2c–e). For each optogenetic system, we quantified the number of clusters formed on illumination and their assembly/disassembly kinetics after illumination changes (see Supplementary Fig. 3). Taken together, our results show that

the assembly and disassembly of membraneless organelles can be robustly triggered with light across a colony of engineered budding yeast cells.

Light-triggered deoxyviolacein flux using optoClusters. The ability to induce the formation of synthetic membraneless organelles could have enormous potential for metabolic engineering, enabling the on-demand compartmentalization of metabolic enzymes and thus control of metabolic flux. To demonstrate this potential in a controlled model system, we set out to control the flux through the deoxyviolacein pathway.

The deoxyviolacein pathway produces two distinct end products depending on the level of activity of two enzymes: VioE and VioC (Supplementary Fig. 4). VioE catalyzes the formation of an intermediate, protodeoxyviolaceinate (PTDV), which is then converted by VioC to the pink-colored product deoxyviolacein. Alternatively, PTDV can be spontaneously oxidized to a green product, prodeoxyviolacein (PDV). Both products, PDV and deoxyviolacein, can be detected by chromatographic methods (Supplementary Fig. 5)[38]. This ease of product quantification makes the deoxyviolacein pathway an ideal platform for assessing metabolic flux control by light-inducible enzyme clustering.

We hypothesized that by inducing the co-localization of VioE and VioC, we could shift flux from PDV to deoxyviolacein production. As a first test of this hypothesis we fused VioE and VioC to the components of our optoCluster system (Fig. 3a). We generated a yeast strain (YNS21) that constitutively expresses VioA and VioB (Supplementary Table 2). We then integrated several copies of a cassette containing VioE-optoCluster and VioC-optoCluster fusions, driven by P_{ADH1}, into δ-sites of YNS21 (see Methods and Supplementary Tables 1 and 2). Both N and C terminal orientations were tested for the optoCluster/enzyme fusions, leading to a total of four yeast strains (YNS34, YNS34-cterm, YNS36, YNS36-cterm) (Supplementary Table 2). We then screened several colonies of each transformation with various $[Zeo]_{max}$ levels for light-dependent changes in PDV production.

The two strains expressing VioE-optoCluster (YNS34-cterm, YNS36-cterm) failed to produce any detectable deoxyviolacein in either light or dark conditions, suggesting that VioE is non-functional with the optoCluster domains fused to its C terminus. However, strains co-expressing optoCluster-VioE and either optoCluster-VioC (YNS34) or VioC-optoCluster (YNS36) exhibit approximately a two-fold increase in deoxyviolacein production and a corresponding decrease in PDV production when incubated under continuous blue light, relative to their production levels in the dark (Fig. 3b–d). The light-induced change in PDV/deoxyviolacein levels is exactly what would be expected in the current model of light-induced enzyme clustering[15]. Inside a cluster, the PTDV intermediate produced by VioE would have an increased likelihood of encountering co-clustered VioC, leading to enhanced deoxyviolacein production. Moreover, this enhanced conversion would reduce steady-state PTDV levels, decreasing the production of the alternative PDV product.

We conducted a series of control experiments to confirm that flux redirection was due to co-clustering of both enzymes rather than a clustering-induced change in the function of VioC or VioE alone. No light-dependent change in product formation was observed in strains expressing VioC-optoCluster and un-clustered VioE, un-clustered VioC and optoCluster-VioE, or VioE and VioC without clustering tags (Fig. 3e and Supplementary Fig. 6). We also verified that the total protein levels of VioC and VioE were not changed by light or dark incubation in either of two VioC/VioE-optoCluster strains (YNS34 and YNS36; Supplementary Fig. 7). Finally, we used live-cell microscopy to verify that VioE-VioC clusters were indeed light-switchable (Fig. 3f). We found that VioE forms constitutive clusters even without light exposure, probably due to synergy between VioE's innate tendency to oligomerize and the FUS^N tag. In contrast, VioC's clustering was light-inducible: VioC was diffuse in the dark, shifting to clusters that co-localized with VioE on light stimulation (Fig. 3f, right panels). Taken together, our results are consistent with a shift in metabolic flux from PDV to deoxyviolacein production driven by enhanced substrate conversion within light-induced VioE-VioC clusters.

We repeated colony screening, light stimulation and deoxyviolacein/PDV product analysis in analogous strains using the optoDroplet system (YNS34drop, YNS36drop) and with Cry2olig-VioC/VioE that lacked the FUS^N tag (YEZ250), but did not observe an increase in deoxyviolacein production under blue light. As the FUS^N tag and Cry2olig variant both serve to increase the extent of light-induced clustering, these data support a model where the strongest-clustering optogenetic variants are best-suited for shifting metabolic flux.

Light-suppressed deoxyviolacein flux using PixELLs. We have seen that light-induced clustering can shift flux toward a desired product on illumination. We next sought to test whether light-dissociated synthetic organelles can invert this response. Light-dissociable enzyme clusters would have the benefit of enhancing flux toward a desired product on a shift from light to darkness, which may be easier to achieve in high-cell-density fermentations and in large-scale bioreactors[33]. Furthermore, having both light-assembled and light-dissociated organelles in the same strain could enable bidirectional control, shifting cells from growth-promoting metabolism to an engineered pathway by changing light conditions[33].

To generate light-dissociable metabolic organelles we turned to PixELL system (Fig. 4a). Starting from YEZ282 (with VioA/VioB in the *LEU2* locus), we integrated one copy of FUS^N-Citrine-PixE-VioE driven by the strong constitutive P_{PGK1} promoter into the *HIS3* locus, and then integrated multiple copies of FUS^N-FusionRed-PixD-VioC into δ-sites to create strain YEZ257 (Fig. 4b). We found that YEZ257 colonies with a $[Zeo]_{max}$ of 1,200 mg l^{-1} exhibited a pronounced metabolic shift between light and dark conditions (Fig. 4c,d), exceeding the fold change observed previously with the optoCluster system. The best colony showed a 6.1 ± 0.9-fold change in deoxyviolacein production and a corresponding decrease in PDV titer (Fig. 4c,d), leading to an 18.4 ± 4.5-fold change in deoxyviolacein-to-PDV ratio from light to dark conditions (Fig. 4e). This effect was not observed for colonies where $[Zeo]_{max}$ was 400, 800 or 1,600 mg l^{-1}, supporting the observation that the photoswitchable response is optimal at intermediate fusion protein expression levels, where light can efficiently assemble/disassemble clusters throughout the cell population.

As in the case of deoxyviolacein-producing optoClusters, we confirmed that these light-dependent changes in metabolic flux reflect the assembly/disassembly of clusters containing VioC and VioE. Strains expressing VioE-only PixELLs in the presence or absence of un-clustered VioC (YEZ512 and YEZ281, respectively) did not exhibit light-dependent changes in PDV production (Fig. 4f and Supplementary Fig. 8, see Methods). The metabolic shift was also not due to light-induced changes in protein expression, as we observed no difference in VioC or VioE expression levels as a function of light stimulus (strains YEZ257 and YEZ281, see Supplementary Fig. 7). We also used live-cell microscopy to confirm that VioE/VioC PixELLs were assembled in the dark and could be dissociated in blue light (Fig. 4g). Time-lapse imaging of strain YEZ257 revealed that blue light stimulation caused VioC to switch from a clustered to a diffuse subcellular distribution (Fig. 4g, left). In contrast, VioE remains clustered in both light and dark conditions (Fig. 4g, right), just as we had observed previously for the optoCluster system (Fig. 3f). Together, these data demonstrate that PixELL-enzyme fusions are a powerful platform

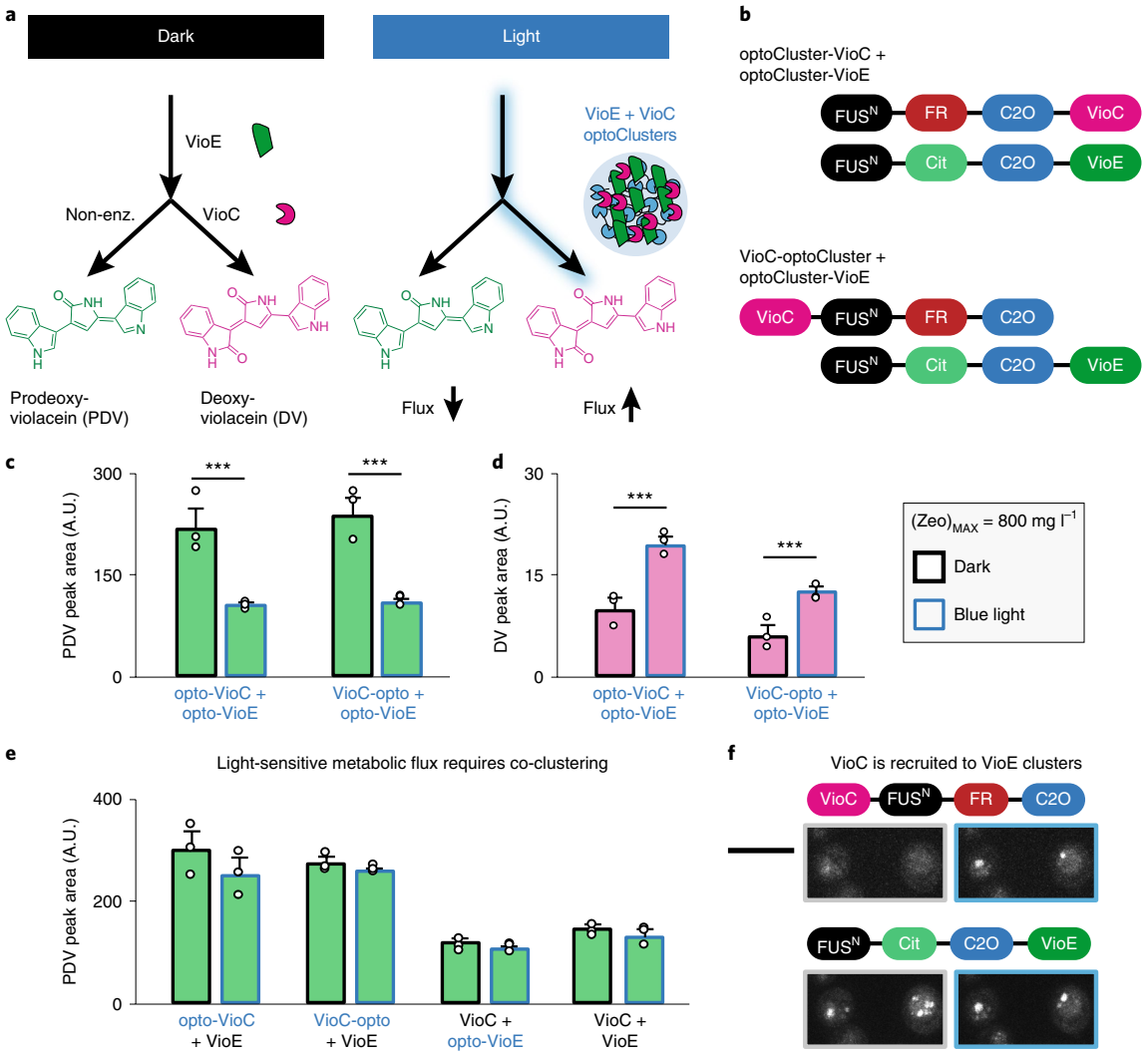

Fig. 3 | Redirecting flux in the deoxyviolacein pathway using light-inducible optoClusters. a, Light-induced co-clustering the VioE and VioC enzymes is expected to increase VioC-induced production of deoxyviolacein (DV) and limit production of PDV. **b**, optoCluster constructs tested for light-induced deoxyviolacein production. **c**,**d**, High-performance liquid chromatography (HPLC) quantification of PDV (**c**) and deoxyviolacein (**d**) from colonies with $[Zeo]_{max} = 800\ mg\ l^{-1}$ (strains YNS34 and YNS36). Cultures were incubated in dark (black outlines) or light (blue outlines) for 4 d before harvesting. ***$P < 0.001$. Statistics are derived using a one-sided *t*-test. **e**, HPLC quantification for PDV in strains lacking co-clustered VioC and VioE (strains YNS54, YNS55, YNS56, YNS57). **f**, Microscopy images of strain YNS34 with $[Zeo]_{max} = 800\ mg\ l^{-1}$, under dark (gray outline) and blue-light conditions (blue outline). Top images indicate FusionRed fluorescence, and bottom images indicate Citrine fluorescence. Images are representative of four colonies picked at the conditions specified and are identically scaled. Scale bar, 5 µm. For the bar graphs in **c** – **e**, error bars represent s.d. of three 1-ml biological replicates (shown as individual points).

for darkness-triggered metabolic flux, complementing the light-triggered flux of optoCluster-enzyme fusions.

One potential limitation of our optogenetic strategy lies in the size of the optogenetic tags, which incorporate a 200 amino acid disordered domain (FUS^N), a fluorescent protein and a light-sensitive domain (for example, the FUS^N-FusionRed-PixD tag is 483 amino acids). We thus tested whether shortened variants might still retain strong light-dependent clustering and metabolic flux enhancement. We found that the FUS^N IDR could be shortened by over 50% to 93 amino acids (termed 'short FUS' or sFUS) while retaining potent light-regulated PixELL clustering (strain YEZ555; Supplementary Fig. 9a). By removing the fluorescent protein, we generated a final sFUS-PixD tag that is approximately half the size of our original tag (247 versus 483 amino acids). The resulting PixELL-expressing strain (YEZ553) was still able to generate a strong light-induced flux shift (Supplementary Fig. 9b–d) and further increased the maximum overall deoxyviolacein yield by 3.2-fold (Supplementary Fig. 9d). These promising improvements suggest that additional gains may be possible through further optimization of the length, IDR sequence, or light-switchable clustering domains[39]. It may also be advantageous to more precisely control the subcellular localization of our optogenetic tools, which are expressed throughout the nucleus and cytosol and can cluster in either compartment (Supplementary Fig. 10). Adding subcellular localization tags (for example, nuclear export sequences or mitochondrial localization tags) could increase yields by limiting clustering to subcellular compartments where the concentration of upstream metabolites is highest.

Light-controlled flux at an enzymatic branch point. Finally, we sought to extend the use of light-controlled metabolic organelles to a more complex scenario. In the deoxyviolacein pathway used so far,

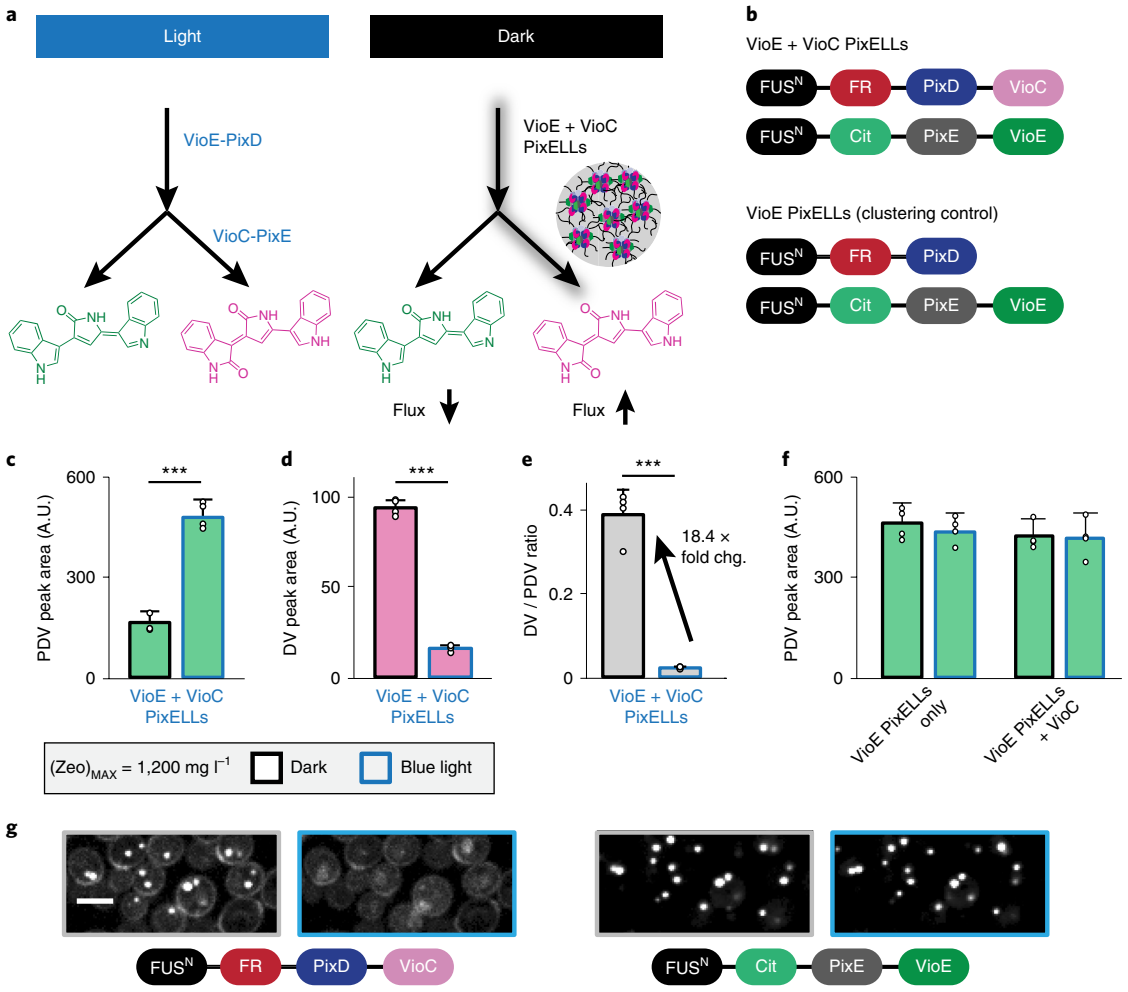

Fig. 4 | Redirecting flux in the prodeoxyviolacein pathway using light-dissociable PixELLs. a, Co-clustering the VioE and VioC enzymes is expected to increase VioC-induced production of deoxyviolacein (DV) and limit production of prodeoxyviolacein (PDV). Because PixELLs are dissociated in the light, this co-clustering enhancement should be lost on light stimulation. **b**, Constructs tested for darkness-induced deoxyviolacein production. **c**–**e**, HPLC quantification of deoxyviolacein (**c**), of PDV (**d**) and of the deoxyviolacein/PDV ratio (**e**) from 4-d fermentations of a YEZ257 colony with $[Zeo]_{max} = 1{,}200\ mg\ l^{-1}$. ***$P < 0.001$. Statistics are derived using a one-sided *t*-test. **f**, HPLC quantification of PDV for four-day fermentations of strains YEZ281 and YEZ512 lacking co-clustered VioE and VioC. **g**, Microscopy images of YEZ257 under different light conditions showing constitutively clustered VioE but light-induced delocalization of VioC. Images are representative of four colonies picked at the conditions specified and are identically scaled. Scale bar, 5 μm. For the bar graphs in **c**–**f**, error bars represent s.d. of four 1-ml biological replicates (shown as individual points).

enzyme-catalyzed deoxyviolacein production competes with a non-enzymatic side pathway. However, many metabolic pathways have branch points where two enzymes compete for access to a single intermediate (Fig. 1a–c), raising the question whether clustering would be effective at such a two-enzyme branch point. We reasoned that such a branch point could be created in our system by adding a single additional enzyme, VioD. VioD competes with VioC for the substrate PTDV, driving the formation of two other pigments: proviolacein and violacein (Fig. 5a).

We expressed VioD driven by the P_{PGK1} promoter from a 2μ plasmid into strain YEZ257, which we previously used to study PixELLs containing VioE/VioC (Fig. 4). Indeed, we found that flux through both enzymatic branches could be switched with light: proviolacein/violacein levels were highest in the light when VioE/VioC PixELLs were dissociated, and deoxyviolacein levels were highest in the dark (Fig. 5b). However, unlike the results obtained from our linear pathway (Figs. 3 and 4), we did not observe a change in PDV levels in the branched-enzyme scenario (Fig. 5b). PDV is produced non-enzymatically from PTDV, so the observation of constant PDV levels suggests that the PTDV intermediate levels are no longer changed by light-triggered clustering. This observation may reflect the balance of two competing effects. VioE-VioC clustering is expected to simultaneously increase the consumption of PTDV by VioC but decrease its encounter frequency with VioD; these two effects may balance such that combined flux through both enzymatic pathways is unchanged.

Taken together, our data demonstrate that the light-induced assembly/disassembly of enzyme-containing membraneless organelles can be used to shunt metabolic flux toward a product of interest and away from competing branches. We observe similar deoxyviolacein results with both light-induced optoClusters and darkness-induced PixELLs, demonstrating that our results are robust to off-target, light-dependent processes such as photo-degradation of metabolites or unintended manipulation of endogenous light-sensitive biochemical reactions. In future studies, the bidirectional control afforded by these two systems could also be useful to enhance different sets of reactions under light and dark conditions, thereby reversibly switching cells between 'growth' and 'production' phases[33].

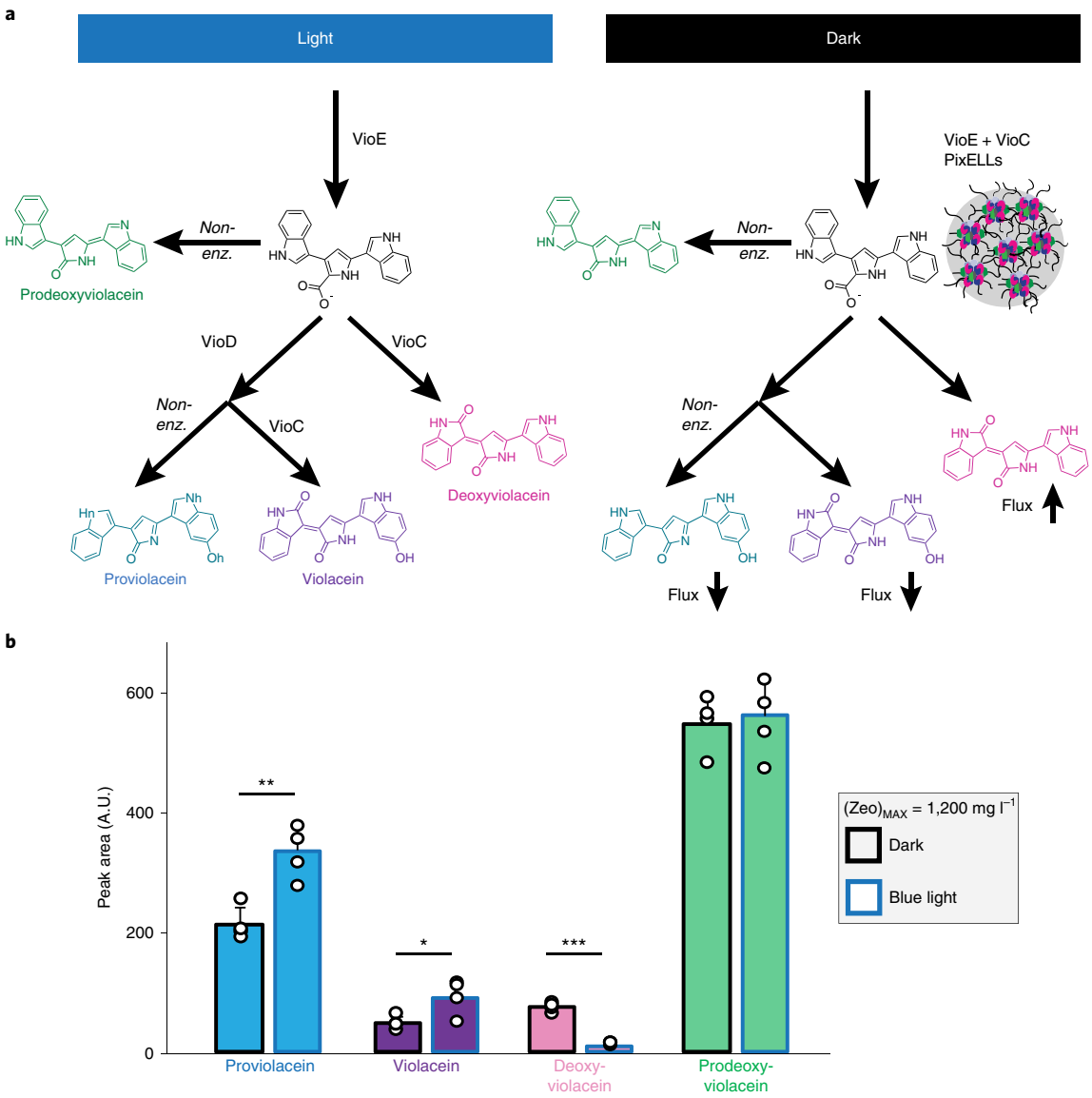

Fig. 5 | Light-switchable metabolic flux control at an enzymatic branch point. a, Co-clustering VioE and VioC is expected to enhance production of deoxyviolacein and suppress an alternative VioD-catalyzed branch that produces proviolacein and violacein. Because PixELLs are dissociated in the light, this co-clustering enhancement should be present in the dark and lost on blue light stimulation. **b**, HPLC quantification of proviolacein, violacein, deoxyviolacein and prodeoxyviolacein from four-day fermentations of strain YEZ511. Error bars represent s.d. of four 1 ml biological replicates (shown as individual points). $^{*}P < 0.05$, $^{**}P < 0.01$, $^{***}P < 0.001$. Statistics are derived using a one-sided *t*-test.

Discussion

Metabolic engineers have previously used physical subcellular compartmentalization for metabolic regulation[22]. Here, we demonstrate that recent advances in light-controlled protein clustering enable us to assemble and disassemble synthetic compartments in yeast. We developed strategies to tune expression levels while mitigating cell-to-cell variability. Using these strategies, we show that two different optogenetic clustering systems achieve light-dependent changes in the formation of violacein pathway products and limit the concentration of intermediate metabolites. Our work thus demonstrates that light-controlled synthetic organelles can indeed be harnessed to dynamically regulate flux through a metabolic pathway.

Nevertheless, developing optogenetic control over enzyme clustering for metabolic engineering is not without its challenges. Reversible clustering activity occurs only at an intermediate range of fusion protein expression levels, and the propensity to cluster can be strongly influenced by fusion to particular metabolic enzymes. For instance, we found that VioE-fused optoClusters and PixELLs exhibit constitutive clustering, even at expression levels that support light-induced assembly/disassembly of VioC clusters. In general, constitutive clustering would be expected for metabolic enzymes such as VioE that exhibit an intrinsic tendency to homo-oligomerize[40].

To address these challenges, we developed a method to sample a wide range of expression levels for our fusion proteins, while also ensuring tight control of expression levels within each transformed colony (Fig. 2). We also established five light-dependent clustering systems for use in budding yeast (Cry2, Cry2olig, optoDroplets, optoClusters and PixELLs) that each have different biophysical properties and that may be optimal for different applications. Additional strategies may prove useful to fine-tune cluster behavior for specific applications, including tuning the density of enzymes within the synthetic organelles (for example, by mixing enzyme-fused and non-enzyme-fused optoClusters in a single cell)[15], making targeted mutations to eliminate a metabolic

enzyme's homo-oligomerization interfaces, or varying the length and sequence of the disordered domain.

Despite these challenges, the use of light-dependent synthetic organelle formation for metabolic control shows considerable promise. The six-fold increase in deoxyviolacein titers that we observe by co-localizing VioC and VioE into PixELLs matches the theoretical maximum enhancement for co-localizing two consecutive enzymes in a metabolic pathway[15], and corresponds to an 18-fold increase in deoxyviolacein-to-PDV production ratio. Moreover, the benefit to pathway efficiency is predicted to increase steeply as the number of co-localized enzymes increases. A theoretical analysis suggests that three-enzyme clusters could exhibit metabolic flux enhancements up to 110-fold relative to the diffuse-enzyme case[15]. Future work that extends controllable enzyme clustering to longer pathways could thus enhance production even more dramatically than what was reported here.

A second important consequence of enzyme co-localization is that the accelerated conversion of pathway intermediates is expected to lower their intracellular steady-state concentration. Complex metabolic pathways often contain intermediates that can be siphoned off to alternative undesirable products, lowering yields[41]. Intermediates may also be toxic; for instance, in the production of the antimalarial drug artemisinin it is vital to prevent accumulation of the toxic intermediate isopentenyl pyrophosphate[16,42]. Our results suggest that optogenetic clustering can lower the overall cellular level of intermediate metabolites produced by the clustered enzymes. Although the PTDV intermediate in our pathway is not amenable to direct quantification, measurements of its auto-oxidized product, PDV, suggest that clustering can drive a two- to three-fold decrease in intracellular PTDV concentration at steady state (Figs. 3c and 4c). Moreover, comparing PDV levels in two variants of the light-switchable violacein pathway, one with an enzymatic branch point and one without (Figs. 4 and 5), suggests that clustering at non-branched steps is most effective for depleting intermediates.

In conclusion, we offer a new method for metabolic flux enhancement using light-inducible enzyme compartmentalization into synthetic organelles. Using deoxyviolacein biosynthesis as a model system, we demonstrate that light-switchable organelles can shift flux in both linear and branched metabolic pathways. Our results reveal not only that optogenetics can be harnessed for post-translational metabolic control, but also that phase separation and aggregation are sufficient to shift metabolic pathway flux, opening the door to a deeper understanding of natural metabolisms as well as new opportunities for metabolic engineering.

Online content

Any methods, additional references, Nature Research reporting summaries, source data, statements of code and data availability and associated accession codes are available at https://doi.org/10.1038/s41589-019-0284-8.

Received: 21 August 2018; Accepted: 1 April 2019;
Published online: 13 May 2019

References

1. Nielsen, J. & Keasling, J. D. Engineering cellular metabolism. *Cell* **164**, 1185–1197 (2016).
2. Keasling, J. D. Manufacturing molecules through metabolic engineering. *Science* **50**, 1355 (2011).
3. Ajikumar, P. K. et al. Isoprenoid pathway optimization for Taxol precursor overproduction in *Escherichia coli*. *Science* **330**, 70–74 (2010).
4. Lalwani, M. A., Zhao, E. M. & Avalos, J. L. Current and future modalities of dynamic control in metabolic engineering. *Curr. Opin. Biotechnol.* **52**, 56–65 (2018).
5. Tomala, K. & Korona, R. Evaluating the fitness cost of protein expression in *Saccharomyces cerevisiae*. *Genome Biol. Evol.* **5**, 2051–2060 (2013).
6. Brockman, I. M. & Prather, K. L. J. Dynamic knockdown of *E. coli* central metabolism for redirecting fluxes of primary metabolites. *Metab. Eng.* **28**, 104–113 (2015).
7. Tan, S. Z. & Prather, K. L. Dynamic pathway regulation: recent advances and methods of construction. *Curr. Opin. Chem. Biol.* **41**, 28–35 (2017).
8. Thomik, T., Wittig, I., Choe, J. Y., Boles, E. & Oreb, M. An artificial transport metabolon facilitates improved substrate utilization in yeast. *Nat. Chem. Biol.* **13**, 1158–1163 (2017).
9. Lin, J. L., Zhu, J. & Wheeldon, I. Synthetic protein scaffolds for biosynthetic pathway colocalization on lipid droplet membranes. *ACS Synth. Biol.* **6**, 1534–1544 (2017).
10. Pedley, A. M. & Benkovic, S. J. A new view into the regulation of purine metabolism: the purinosome. *Trends Biochem. Sci.* **42**, 141–154 (2017).
11. French, J. B. et al. Spatial colocalization and functional link of purinosomes with mitochondria. *Science* **351**, 733–737 (2016).
12. Zhang, Y. et al. Protein–protein interactions and metabolite channelling in the plant tricarboxylic acid cycle. *Nat. Commun.* **8**, 15212 (2017).
13. Narayanaswamy, R. et al. Widespread reorganization of metabolic enzymes into reversible assemblies upon nutrient starvation. *Proc. Natl Acad. Sci. USA* **106**, 10147–10152 (2009).
14. Kistler, H. C. & Broz, K. Cellular compartmentalization of secondary metabolism. *Front. Microbiol.* **6**, 1–11 (2015).
15. Castellana, M. et al. Enzyme clustering accelerates processing of intermediates through metabolic channeling. *Nat. Biotechnol.* **32**, 1011–1018 (2014).
16. George, K. W. et al. Integrated analysis of isopentenyl pyrophosphate (IPP) toxicity in isoprenoid-producing *Escherichia coli*. *Metab. Eng.* **47**, 60–72 (2018).
17. Dueber, J. E. et al. Synthetic protein scaffolds provide modular control over metabolic flux. *Nat. Biotechnol.* **27**, 753–759 (2009).
18. Li, T., Chen, X., Cai, Y. & Dai, J. Artificial Protein Scaffold System (AProSS): an efficient method to optimize exogenous metabolic pathways in *Saccharomyces* cerevisiae. *Metab. Eng.* **49**, 13–20 (2018).
19. Lau, Y. H., Giessen, T. W., Altenburg, W. J. & Silver, P. A. Prokaryotic nanocompartments form synthetic organelles in a eukaryote. *Nat. Commun.* **9**, 1311 (2018).
20. Avalos, J. L., Fink, G. R. & Stephanopoulos, G. Compartmentalization of metabolic pathways in yeast mitochondria improves the production of branched-chain alcohols. *Nat. Biotechnol.* **31**, 335–341 (2013).
21. DeLoache, W. C., Russ, Z. N. & Dueber, J. E. Towards repurposing the yeast peroxisome for compartmentalizing heterologous metabolic pathways. *Nat. Commun.* **7**, 11152 (2016).
22. Hammer, S. K. & Avalos, J. L. Harnessing yeast organelles for metabolic engineering. *Nat. Chem. Biol.* **13**, 823–832 (2017).
23. Toettcher, J. E., Voigt, Ca, Weiner, O. D. & Lim, Wa The promise of optogenetics in cell biology: interrogating molecular circuits in space and time. *Nat. Methods* **8**, 35–38 (2011).
24. Shin, Y. et al. Spatiotemporal control of intracellular phase transitions using light-activated optoDroplets. *Cell* **168**, 159–171.e14 (2017).
25. Dine, E., Gil, A. A., Uribe, G., Brangwynne, C. P. & Toettcher, J. E. Protein phase separation provides long-term memory of transient spatial stimuli. *Cell Syst.* **6**, 655–663 (2018).
26. Taslimi, A. et al. An optimized optogenetic clustering tool for probing protein interaction and function. *Nat. Commun.* **5**, 4925 (2014).
27. Nakamura, H. et al. Intracellular production of hydrogels and synthetic RNA granules by multivalent molecular interactions. *Nat. Mater.* **17**, 79–88 (2018).
28. Bugaj, L. J., Choksi, A. T., Mesuda, C. K., Kane, R. S. & Schaffer, D. V. Optogenetic protein clustering and signaling activation in mammalian cells. *Nat. Methods* **10**, 249–252 (2013).
29. Gil, A. A. et al. Photoactivation of the BLUF protein PixD probed by the site-specific incorporation of fluorotyrosine residues. *J. Am. Chem. Soc.* **139**, 14638–14648 (2017).
30. Shemiakina, I. I. et al. A monomeric red fluorescent protein with low cytotoxicity. *Nat. Commun.* **3**, 1204 (2012).
31. Shin, Y. & Brangwynne, C. P. Liquid phase condensation in cell physiology and disease. *Science* **357**, eaaf4382 (2017).
32. Yuan, J. & Ching, C. B. Combinatorial assembly of large biochemical pathways into yeast chromosomes for improved production of value-added compounds. *ACS Synth. Biol.* **4**, 23–31 (2014).
33. Zhao, E. M. et al. Optogenetic regulation of engineered cellular metabolism for microbial chemical production. *Nature* **555**, 683–687 (2018).
34. Yuan, H. & Bauer, C. E. PixE promotes dark oligomerization of the BLUF photoreceptor PixD. *Proc. Natl Acad. Sci. USA* **105**, 11715–11719 (2008).
35. Brachmann, C. B. et al. Designer deletion strains derived from *Saccharomyces cerevisiae* S288C: a useful set of strains and plasmids for PCR-mediated gene disruption and other applications. *Yeast* **14**, 115–132 (1998).
36. Giaever, G. & Nislow, C. The yeast deletion collection: a decade of functional genomics. *Genetics* **197**, 451–465 (2014).

37. Entian, K. D. & Kötter, P. 25 Yeast genetic strain and plasmid collections. *Meth. Microbiol.* **36**, 629–666 (2007).
38. Lee, M. E., Aswani, A., Han, A. S., Tomlin, C. J. & Dueber, J. E. Expression-level optimization of a multi-enzyme pathway in the absence of a high-throughput assay. *Nucleic Acids Res.* **41**, 10668–10678 (2013).
39. Bracha, D. et al. Mapping local and global liquid phase behavior in living cells using photo-oligomerizable seeds. *Cell* **175**, 1467–1480.e13 (2018).
40. Ryan, K. S., Balibar, C. J., Turo, K. E., Walsh, C. T. & Drennan, C. L. The violacein biosynthetic enzyme VioE shares a fold with lipoprotein transporter proteins. *J. Biol. Chem.* **283**, 6467–6475 (2008).
41. Martin, V. J. J., Pitera, D. J., Withers, S. T., Newman, J. D. & Keasling, J. D. Engineering a mevalonate pathway in *Escherichia coli* for production of terpenoids. *Nature* **21**, 796–802 (2003).
42. Ro, D. et al. Production of the antimalarial drug precursor artemisinic acid in engineered yeast. *Nature* **440**, 3–6 (2006).

Acknowledgements

We thank all members of the Toettcher and Avalos laboratories for helpful comments. We also thank J. Dueber for kindly providing violacein enzyme plasmids. This work was supported by the Maeder Graduate Fellowship in Energy and the Environment (to E.M.Z.), NIH grant DP2EB024247 (to J.E.T.) and The Pew Charitable Trusts, the U.S. DOE Office of Biological and Environmental Research, Genomic Science Program Award DESC0019363, and NSF CAREER Award CBET-1751840 (to J.L.A.) and a Schmidt Transformative Technology grant (to J.E.T. and J.L.A).

Author contributions

E.M.Z., M.Z.W., J.E.T. and J.L.A. conceived the project and designed the experiments. E.M.Z. and N.S. conducted all metabolic flux experiments. E.M.Z., N.S., M.Z.W., E.D. and N.L.P. cloned constructs and performed microscopy. Z.G. contributed methodology and reagents. E.M.Z., J.E.T. and J.L.A. wrote the paper with editing from all authors. J.E.T. and J.L.A. provided funding and supervised the research.

Competing interests

Some of the authors are co-inventors on patent applications harnessing optogenetics for metabolic engineering (J.L.A., J.E.T. and E.M.Z.: patent application no. WO2017177147A1) and establishing optogenetic control of protein clustering (J.E.T.: patent application no. US20170355977A1).

Additional information

Supplementary information is available for this paper at https://doi.org/10.1038/s41589-019-0284-8.

Reprints and permissions information is available at www.nature.com/reprints.

Correspondence and requests for materials should be addressed to J.L.A. or J.E.T.

Publisher's note: Springer Nature remains neutral with regard to jurisdictional claims in published maps and institutional affiliations.

Methods

Assembly of DNA constructs. Ligations and one-step isothermal assembly reactions were conducted using previously described methods[33]. Cry2 and PixELL constructs were obtained from previously published sources (Addgene constructs 111507, 111506 and 111503) and amplified using PCR with similarity arms for Gibson assembly[24,25]. Backbones were either amplified by PCR or cut using available enzymes from the pJLA vector system[20]. All constructs were sequenced by Genewiz (Supplementary Table 1). Sequences of optogenetic systems are available in Supplementary Sequences.

Strain construction and descriptions. Further description of the constructs and strains described below can also be found in Supplementary Tables 1 and 2 and Supplementary Fig. 11.

Construction of optoDroplet, optoCluster and PixELL-expressing strains. To create optoDroplet and optoCluster strains, we integrated multiple copies of constructs containing different combinations of FUS^N, Cry2 and Cry2olig (pNS1, pNS2, pNS3, pNS4) fused to fluorescent proteins and selected on increasing levels of zeocin (400, 800, 1,200 and 1,600 mg l^{-1}, which corresponded to an increasing number of integration events). The resulting strains are YNS47, YNS48, YNS49 and YNS50, respectively. We observed that only constructs with the FUS^N tag (pNS1, pNS3) formed visible phase-separated bodies when induced with light. To construct PixELL-expressing strains, we integrated a single copy of FUS^N-Citrine-PixE (EZ-L498 to make YEZ231) into the *HIS3* locus and multiple copies of FUS^N-FusionRed-PixD (EZ-L499 to make YEZ232, selected on 1,200 mg l^{-1} zeocin) into the δ-sites in the yeast genome. No phase separation was observed when only one component, PixD or PixE alone, was used (YEZ234).

Screening of other clustering constructs. To test other light-inducible clustering tags, we constructed plasmids pNP1-Drop, pNP3-Drop, pNP7 and EZ-L477. These plasmids represent all combinations of fusions of FUS^N-FusionRed-Cry2 and FusionRed-Cry2olig with either VioE or VioC. We screened 24 colonies of YNS21 + pNP1-Drop + pNP3-Drop (YNS34drop), 24 colonies of YNS21 + pNP2-Drop + pNP3-Drop (YNS36drop) and 24 colonies of YNS21 + pNP7 + EZ-L477 (YEZ250). None of these combinations yielded a higher production of deoxyviolacein in the light than in the dark.

Why might optoClusters and PixELLs exhibit strong metabolic shifts while optoDroplets do not? One possibility is that optoDroplets exhibit weaker light-switchable clustering and thus total enzyme redistribution. The optoCluster system includes an additional point mutation that favors Cry2 oligomerization and clustering. Also, the PixELL system is made up of two Pix proteins, so whichever of the two is limiting in expression tends to exhibit near-complete redistribution in/out of clusters. These differences could lead optoDroplets to have a lower total shift from a diffuse to clustered enzyme distribution.

A second possibility is that although variability is low within a colony, the expression levels (and thus, number of clusters) of the optogenetic tools can still vary substantially between colonies. By screening more than 24 colonies or testing additional $[Zeo]_{max}$ values, it may be still be possible to optimize optoDroplet-enzyme expression to shift metabolic flux.

Deoxyviolacein pathway control using optoClusters. We constitutively expressed VioA and VioB by integrating pNS5 into BY4741 to generate YNS21. Using δ-integration, we then expressed a VioC (pNP1 or pNP2) and a VioE (pNP3 or pNP4) plasmid, both fused to FUS^N-Cry2olig tags at either the N or C termini, in all possible combinations for a total of four yeast constructs (see Methods and Supplementary Tables 1 and 2). This made strains YNS34 (pNP1, pNP3), YNS34-cterm (pNP1, pNP4), YNS36 (pNP2, pNP3) and YNS36-cterm (pNP2, pNP4). After selecting in 800 mg l^{-1} of zeocin and screening multiple colonies of each combination, we observed an increased production of deoxyviolacein relative to PDV in response to light activation in strains YNS34 and YNS36.

Deoxyviolacein pathway control using PixEL. To redirect flux toward deoxyviolacein with the PixELL system, we integrated EZ-L528 (for expression of VioA and VioB, required to produce the IPA imine dimer precursor metabolite from tryptophan; see Supplementary Figure 3 and Tables 1 and 2) into BY4741 to make YEZ282. We then integrated one copy of a FUS^N-Citrine-PixE-VioE fusion (EZ-L526) under a strong, constitutive promoter, P_{PGK1}, to make YEZ255. We expressed various levels (at 400, 800, 1,200 and 1,600 mg l^{-1} of zeocin) of a FUS^N-FusionRed-PixD-VioC fusion (EZ-L527) by using δ-integration (YEZ257, Fig. 4b, see Supplementary Tables 1 and 2). For colonies where $[Zeo]_{max}$ = 1,200 mg l^{-1}, we observed a higher level of deoxyviolacein production when the culture was grown in the dark than when the deoxyviolacein production when the same culture was grown in the light (Fig. 4c). The best colony showed a 6.1-fold change from light to dark conditions with consistent decreases in PDV titer (Fig. 4d). This effect was not observed for colonies where $[Zeo]_{max}$ was 400, 800 or 1,600 mg l^{-1} of zeocin. We controlled for the effects of clustering by integrating EZ-L499 into YEZ255, resulting in YEZ281, a strain that clusters PixD and PixE on blue light stimulation but lacks VioC and thus produces no deoxyviolacein. We also added pNS7 to YEZ281 to control for constitutive non-localizing VioC control, making YEZ512.

Diverting flux away from VioD using PixELLs. To test the effect of the PixELL system on a metabolic branch point containing a competing enzyme, we added VioD to the existing system. We added EZ-L859 to YEZ257 to make YEZ511. We saw that in YEZ511, the entire system produced more products of the violacein pathway (PDV, deoxyviolacein, proviolacein and violacein). However, we also saw the intended effect, which was a shift from more deoxyviolacein production in the light to more proviolacein and violacein production in the dark. This dependence on light condition of proviolacein and violacein production was not seen in our control strains.

Shortening the FUS^N tag for diverting flux using PixELLs. As the size of the tags are large and could complicate protein activity and/or expression, we tested a tag of reduced size for chemical production. We did this by first limiting the size of the FUS^N domain to the first 93 amino acids. We named this iteration sFUS. We first tested to see how sFUS functions with fluorescent proteins. We added EZ-L767 (sFUS-FR-PixD) to YEZ231 and selected on 1,200 mg l^{-1} of zeocin to make YEZ555. We then wanted to test minimizing the tag on deoxyviolacein production. We did this by both shortening FUS to sFUS and removing the fusion red protein from the VioC expression construct. We integrated EZ-L786 into YEZ255 to make YEZ553 and selected on 1,200 mg l^{-1} of zeocin to make YEZ553. We controlled for the effects of clustering by integrating EZ-L767 into YEZ255, resulting in YEZ554, a strain that clusters PixD and PixE on blue light stimulation but lacks VioC and thus produces no deoxyviolacein.

Yeast strains and transformations. Strain transformations were carried out using standard lithium acetate protocols. For zeocin selection assays, the DNA added was varied between 100 µg and 3 mg per transformation depending on the target zeocin concentration[32,33]. For experiments with a target $[Zeo]_{max}$ = 400 mg l^{-1}, we transformed 70 µl of competent cells using 100 µg of DNA; for $[Zeo]_{max}$ = 800 mg l^{-1}, we transformed them with 500 µg of DNA; for $[Zeo]_{max}$ = 1,200 mg l^{-1}, we used 1.5 mg of DNA and for $[Zeo]_{max}$ = 1,600 mg l^{-1}, we transformed 3 mg of DNA. Colonies were grown on both the $[Zeo]_{max}$ concentration and one level higher (800 mg l^{-1} for $[Zeo]_{max}$ = 400 mg l^{-1}). Colonies that appear on the $[Zeo]_{max}$ concentration plate but not on the higher concentration plate were selected as colonies with that $[Zeo]_{max}$.

Fluorescence microscopy. To prepare culture for microscopy, yeast strains were cultured overnight at 30 °C from a single colony, in the appropriate synthetic complete media with 2% glucose (for example, SC-ura + 2% glucose for a strain that contained a *URA3* plasmid), in a 24-well plate covered with aluminum foil. Synthetic media was used to avoid the high auto-fluorescence of yeast extract peptone dextrose (YPD) media. The following day, cultures were diluted 1:20 and allowed to grow for 2 h at 30 °C. Wells of a 96-well glass-bottomed plate (Sigma CLS4580) were coated with 50 µl of 1 mg ml^{-1} Concanavalin A (Sigma) dissolved in 20 mM sodium acetate. After washing wells with ddH2O, yeast cultures were transferred and spun down at 1,000 r.p.m. for 3 min. All imaging was carried out using a 60× oil immersion objective (numerical aperture 1.4) on a Nikon TI Eclipse microscope with a CSU-X1 confocal spinning disk, an EM-CCD camera and appropriate laser lines, dichroics and filters. Blue light photoactivation was carried out by exciting with a 488 nm laser line or illumination from a 450 nm light-emitting diode (LED). To quantify the kinetics of cluster assembly/disassembly (Supplementary Fig. 3) we measured the background-subtracted mean, µ, and s.d., σ, of pixel intensities within each cell and at each timepoint. We then calculated the signal-to-noise ratio (SNR) of pixel intensities (defined as SNR = µ/σ), a sensitive and reproducible metric reflecting the extent of clustering[25].

Analysis of cluster number and assembly/disassembly kinetics. We observed light-dependent organelle formation in yeast made to express three of our optogenetic systems: optoClusters, optoDroplets and PixELLs. Yet, in each of these cases, the extent and timescale of clustering differed, an observation that we sought to describe more quantitatively using live-cell imaging in each case. We imaged yeast strains YNS47 (optoDroplets), YNS49 (optoClusters) and YEZ232 (PixELLs) in the FusionRed channel during cycles of 450 nm blue light illumination or darkness. We then quantified the extent of clustering by analyzing the number of clusters per cell and the kinetics of cluster assembly/disassembly using changes in the pixel-to-pixel SNR, which measures the homogeneity of cluster intensities (that is, lower SNR = more clustering). We found that on average we observed between 1 – 4 clusters per cell across these three systems, with fewer PixELLs and OptoDroplets per cell and more optoClusters per cell under clustering conditions (Supplementary Fig. 3a). However, the number of clusters certainly depends on a large number of parameters, including the length of time of clustering (due to processes such as ripening and fusion events) and the expression level of the constructs, so these results should be taken as indicative of results in our conditions, not universal properties of these optogenetic tools.

We also measured the kinetics of cluster assembly/disassembly, observing fast light-induced changes in all three systems. These changes worked in opposing directions depending on the optogenetic system used. For instance, we observed light-induced assembly over ~5 min in optoCluster/optoDroplet cells (Supplementary Fig. 3b,c), and light-induced disassembly within 30 s in PixELL-expressing cells (Supplementary Fig. 3d). In contrast, dark-induced reversion occurs on different timescales for each optogenetic system: PixD switches back to its dark-state conformation with a half-life of ~5 s (ref. [43]), whereas Cry2 switches back in ~2 min and Cry2olig in ~20 min (ref. [26]). Matching these optogenetic dark-state kinetics, we found that Cry2-based optoDroplets dissociated in minutes, Cry2olig-based optoClusters were not fully dissociated even after 30 min in the dark and PixD-based PixELLs reassembled in minutes after dark incubation (Supplementary Fig. 3b – d).

Assessing and correcting for violacein product photobleaching. An optogenetic system requires continuous illumination with blue light that raises the possibility of light-induced photobleaching or degradation. To measure the photobleaching and/or degradation of PDV, deoxyviolacein, proviolacein and violacein under blue light stimulation, we measured the production of PDV, deoxyviolacein, proviolacein and violacein in strains constitutively expressing violacein enzymes without optogenetic control (YNS51, MZW342, MZW375, MZW377 and MZW378) under lit and dark conditions. In four of these strains (MZW342, MZW375, MZW377 and MZW378), expression of the violacein pathway enzymes was under the control of a β-estradiol inducibler promoter. We thus added β-estradiol to a final concentration of 1 μM throughout the fermentation[1]. For all light stimulation experiments we used the same blue light source under identical conditions.

We found that deoxyviolacein is degraded slowly and at a constant rate by blue light, so that illuminated samples always exhibited a proportionally smaller deoxyviolacein peak by high-performance liquid chromatography (HPLC) (Supplementary Fig. 5). Individual points represent YNS51, MZW342, MZW375, MZW377 and MZW378, five strains with different deoxyviolacein production levels. We thus normalized all deoxyviolacein measurements taken after blue light illumination using the standard curve produced by these control strains (Supplementary Fig. 5). We observed no photobleaching by blue light for PDV, proviolacein or violacein in these assays. No differences in growth rate or maximum optical density were observed from these strains when cultured in the light or dark.

Light panel set ups. All light illumination for fermentations were carried out with blue LED panels (HQRP New Square 12" Grow Light Blue 517 LED 14 W), placed 40 cm from cell cultures. At these heights, the light panel outputs ranged from 73 μmoles per m^2 per s to 82 μmoles per m^2 per s, on the basis of measurements taken using a quantum meter (Model MQ-510 from Apogee Instruments).

Yeast fermentations. Eight colonies were chosen from each zeocin selection plate for optoCluster and PixELL fermentations to screen for deoxyviolacein and PDV production. Each colony's $[Zeo]_{max}$ was noted and the colony was saved for future use by plating onto an agar plate. Colonies were used to inoculate 1 ml of SC-his + 2% glucose media in 24-well plates and grown overnight at 30 °C, 200 r.p.m., and under ambient light conditions. Each culture was then diluted into two different plates and grown for 20 h, with one plate grown under continuous blue light and the other wrapped in tinfoil and grown in the dark. Each culture was then centrifuged at 1,000 r.p.m. for 5 min under ambient light and cell pellets were resuspended in 1 ml of fresh SC-his + 2% glucose media. The plates were then incubated under their respective light conditions for 96 h at 30 °C. Each 1 ml sample was then transferred to a 1.5 ml microcentrifuge tube and centrifuged at 1,000 r.p.m. for 10 min under ambient light. The supernatants were discarded and pellets were then resuspended in 1 ml of methanol (see the section Extraction and Quantification of Deoxyviolacein-Pathway Products). After identification of the colonies exhibiting the highest light-dependent fold change in metabolic yield, four replicates of the best colonies were then conducted and quantified using the same protocol.

Extraction and quantification of deoxyviolacein-pathway products. To quantify the deoxyviolacein, PDV, proviolacein and violacein produced by the fermentations, the cell pellets obtained from centrifuging 1 ml fermentation samples (see the section Yeast Fermentations) were resuspended in 1 ml of 100% methanol and incubated at 95 °C for 15 min, vortexing for 2 – 5 s halfway through. Cells were then centrifuged at 13,000 r.p.m. for 5 min and approximately 800 μl of supernatant was transferred to a new microcentrifuge tube. The new microcentrifuge tube was again centrifuged at the same conditions and transferred to HPLC vials for analysis. Filtration of extracts was avoided because products are trapped by the filter membrane. Extracts were run on an Alltech Alltima C18 column (250 × 4.6 mm, 5 μm particle size) on an Agilent 1200 Series LC system using 0.1% trifluoroacetic acid in acetonitrile (Solvent A), 0.1% trifluoroacetic acid in water (Solvent B) and the following method: start at 5% Solvent A; from 0 – 10 min, linear increase of Solvent A from 5 to 95%; hold at 95% Solvent A from 10 – 13 min; Linear decrease of Solvent A from 95 to 5% A from 13 – 13.5 min. The flow rate was 0.9 ml per min and products were monitored with an Agilent diode array detector at 565 nm. Product identities were confirmed using an Agilent 6120 Quadrupole mass spectrometer, using electrospray ionization in positive mode. Retention times were 10.04 min for proviolacein (*m/z* [M + H] + of 328), 10.84 min for prodeoxyviolacein (*m/z* [M + H] + of 312), 10.95 min for violacein (*m/z* [M + H] + of 344) and 12.25 min for deoxyviolacein (*m/z* [M + H] + of 328).

Normalization for photobleaching of deoxyviolacein. To normalize for the degradation of any violacein pathway product under blue light, we conducted fermentation and product analysis on five strains that produced constant amounts of deoxyviolacein-pathway chemicals: MZW342, MZW375, MZW377, MZW378 and YNS51 (Supplementary Table 2). Concentrations of deoxyviolacein, PDV, proviolacein and violacein were measured for cultures that were fermented under identical conditions except in either blue light or in the dark. These fermentations mimicked the ones we carried out to control assembly or disassembly of synthetic organelles—96 h of fermentations after resuspension in new media. Although PDV, proviolacein and violacein levels were consistent for dark and light conditions, deoxyviolacein exhibited substantial but consistent degradation under blue light (Supplementary Fig. 5). Least-squares regression of the data reveals that deoxyviolacein measurements of samples fermented under blue light scaled linearly deoxyviolacein measurements of samples fermented in the dark. To compensate for this degradation, we corrected all deoxyviolacein measurements for cultures fermented under blue light by a factor of 3.453.

Measurement of fluorescence protein levels. To measure the protein concentrations of the relevant clustered enzymes, we grew cells from each of YEZ281, YEZ257, YNS34 and YNS36 in liquid SC-his overnight in the dark (tin-foil covered). Each culture was then diluted into two different plates in quadruplicates to 0.1 optical density (OD_{600}) in fresh SC-his and grown for 20 h, with one plate grown under continuous blue light and the other wrapped in tinfoil and grown in the dark. Each culture was then centrifuged at 1,000 r.p.m. for 5 min under ambient light and cell pellets were resuspended in 1 ml of fresh SC-his + 2% glucose media.

The plates were then incubated under their respective light conditions for 96 h at 30 °C. Cells were then diluted 1:10 into fresh SC-his + 2% glucose media. Fluorescence and OD_{600} measurements were taken using a TECAN plate reader (infinite M200PRO). The excitation and emission wavelengths used for Citrine fluorescence measurements were 485 and 535 nm, respectively, using an optimal gain for all measurements. The excitation and emission wavelengths used for FusionRed fluorescence measurements were 570 and 615 nm, respectively. To process fluorescence data, the background fluorescence from the media was first subtracted from all pixel values. Then, the fluorescence/OD_{600} values of cells lacking a fluorescence protein construct were subtracted from the fluorescence values (fluorescence/OD_{600}) of each sample to normalize for light bleaching of the media and cell contents. Thus, reported values were calculated according to the following formula.

$$\text{Fluorescence}/\text{OD}_{\text{Strain,Condition}} = \frac{(\text{Fluorescence}_{\text{Strain,Condition}} - \text{Fluorescence}_{\text{Media,Condition}})}{(\text{OD}_{\text{Strain,Condition}} - \text{OD}_{\text{Media,Condition}})} - \frac{(\text{Fluorescence}_{\text{No GFP Control Strain,Condition}} - \text{Fluorescence}_{\text{Media,Condition}})}{(\text{OD}_{\text{No GFP Control Strain,Condition}} - \text{OD}_{\text{Media,Condition}})}$$

YEZ140 was used as the no-fluorescence control. All fluorescence measurements were done at the end of experiments or on samples taken from experimental cultures.

Yeast cell fixing and staining with 4′,6-diamidino-2-phenylindole (DAPI). We previously found that PixeLLs and optoDroplets/optoClusters show an increased propensity to cluster in the nucleus of mammalian cells[24,25], raising the possibility that light-controlled clusters are also predominantly localized to the nucleus in yeast. To determine whether this was the case, we set out to fix and stained PixELL-expressing cells and co-stained them with DAPI to mark the cell nucleus.

Yeast strains YEZ232 and YEZ555 were inoculated into SC-his + 2% glucose medium and grown to an OD_{600} of 2. From these cultures, 900 μl was transferred to a 1.5 ml microcentrifuge tube containing 100 μl of 37% (w/v) formaldehyde. This mixture was incubated at room temperature for 90 min before spinning down at 7,500*g* for 1 min and washing with 0.3 ml of Dulbecco's phosphate-buffered saline (DPBS) solution two times. After resuspension in 0.3 ml of DPBS, 0.7 ml of 200 Proof ethanol was added to permeabilize and incubated at room temperature for 30 min. Cells were then spun down again and resuspended in 300 μl of DPBS, diluted ten-fold into new DPBS and mixed 1:1 with 100 ng ml^{-1} DAPI in DPBS solution. Cells were then plated and imaged on the basis of our standard microscopy procedure (see the Fluorescence Microscopy section).

Statistics. Statistical significance was determined using a standard *t*-test for *P* values. *T* scores were calculated by the formula:

$$\frac{(\text{Mean}_{\text{Condition 2}} - \text{Mean}_{\text{Condition 1}})\sqrt{\text{Number of samples}}}{\text{Standard Deviation}_{\text{Condition 2}}}.$$

P values were calculated using three degrees of freedom and a one-sided *t*-test calculator.

Reporting Summary. Further information on research design is available in the Nature Research Reporting Summary linked to this article.

Data availability

All plasmids, strains and raw data will be made available upon reasonable request to the corresponding authors.

References

43. Hua Yuan, H. et al. Mutational and Structural Studies of the PixD BLUF Output Signal That Affects Light-Regulated Interactions with PixE. *Biochemistry* **50**, 6365 – 6375 (2011).

nature research

Corresponding author(s): Jared E. Toettcher and José L. Avalos

Reporting Summary

Nature Research wishes to improve the reproducibility of the work that we publish. This form provides structure for consistency and transparency in reporting. For further information on Nature Research policies, see Authors & Referees and the Editorial Policy Checklist.

Statistical parameters

When statistical analyses are reported, confirm that the following items are present in the relevant location (e.g. figure legend, table legend, main text, or Methods section).

n/a	Confirmed	
☐	☒	The exact sample size (*n*) for each experimental group/condition, given as a discrete number and unit of measurement
☐	☒	An indication of whether measurements were taken from distinct samples or whether the same sample was measured repeatedly
☒	☐	The statistical test(s) used AND whether they are one- or two-sided *Only common tests should be described solely by name; describe more complex techniques in the Methods section.*
☒	☐	A description of all covariates tested
☐	☒	A description of any assumptions or corrections, such as tests of normality and adjustment for multiple comparisons
☐	☒	A full description of the statistics including central tendency (e.g. means) or other basic estimates (e.g. regression coefficient) AND variation (e.g. standard deviation) or associated estimates of uncertainty (e.g. confidence intervals)
☐	☒	For null hypothesis testing, the test statistic (e.g. *F*, *t*, *r*) with confidence intervals, effect sizes, degrees of freedom and *P* value noted *Give P values as exact values whenever suitable.*
☒	☐	For Bayesian analysis, information on the choice of priors and Markov chain Monte Carlo settings
☒	☐	For hierarchical and complex designs, identification of the appropriate level for tests and full reporting of outcomes
☒	☐	Estimates of effect sizes (e.g. Cohen's *d*, Pearson's *r*), indicating how they were calculated
☐	☒	Clearly defined error bars *State explicitly what error bars represent (e.g. SD, SE, CI)*

Our web collection on statistics for biologists may be useful.

Software and code

Policy information about availability of computer code

Data collection	n/a
Data analysis	Microsoft Excel

For manuscripts utilizing custom algorithms or software that are central to the research but not yet described in published literature, software must be made available to editors/reviewers upon request. We strongly encourage code deposition in a community repository (e.g. GitHub). See the Nature Research guidelines for submitting code & software for further information.

Data

Policy information about availability of data

All manuscripts must include a data availability statement. This statement should provide the following information, where applicable:

- Accession codes, unique identifiers, or web links for publicly available datasets
- A list of figures that have associated raw data
- A description of any restrictions on data availability

We have a section stating "The authors declare that all data supporting the findings of this study are available within the paper (and its Supplementary Information files), but original data that supports the findings are available from the corresponding authors upon reasonable request."

Field-specific reporting

Please select the best fit for your research. If you are not sure, read the appropriate sections before making your selection.

☒ Life sciences ☐ Behavioural & social sciences ☐ Ecological, evolutionary & environmental sciences

For a reference copy of the document with all sections, see nature.com/authors/policies/ReportingSummary-flat.pdf

Life sciences study design

All studies must disclose on these points even when the disclosure is negative.

Sample size	Methods Section, n > or = 3 of biological replicates. This is a standard in the field.
Data exclusions	All data presented are from the most recent set of experiments performed. We did not exclude any data from the same experiments.
Replication	All experimental findings are reliably reproduced. We have reproduced each experiment at least twice to ensure reliability.
Randomization	All samples in the same experimental group were biological replicates (same genetic makeup but different origin).
Blinding	Investigators were blind to the group allocation during data acquisition and analysis.

Reporting for specific materials, systems and methods

Materials & experimental systems

n/a	Involved in the study
☒	☐ Unique biological materials
☒	☐ Antibodies
☐	☒ Eukaryotic cell lines
☒	☐ Palaeontology
☒	☐ Animals and other organisms
☒	☐ Human research participants

Methods

n/a	Involved in the study
☒	☐ ChIP-seq
☒	☐ Flow cytometry
☒	☐ MRI-based neuroimaging

Eukaryotic cell lines

Policy information about cell lines

Cell line source(s)	Yeast, Saccharomyces cerevisiae, CEN.PK2-1C and BY4741.
Authentication	Cell lines were not authenticated.
Mycoplasma contamination	Cell lines were not tested for mycoplasma contamination.
Commonly misidentified lines (See ICLAC register)	n/a